Particle & Particle Systems Characterization
www.particle-journal.com

Colloidal Analysis of Particles Extracted from Microalloyed Steels

*Andreas Hegetschweiler, Aljosha-Rakim Jochem, Anna Zimmermann, Johannes Walter, Thorsten Staudt, and Tobias Kraus**

Different colloidal particle characterization methods are examined for their suitability to determine the particle size distribution of particles extracted from steels. Microalloyed steels are dissolved to extract niobium and titanium carbonitride particles that are important for the mechanical properties of these steels. Such particles have sizes ranging from several nanometers to hundreds of nanometers depending on the precipitation stage during the thermomechanically controlled rolling process. The size distribution of the particles is analyzed by dynamic light scattering (DLS), analytical ultracentrifugation (AUC), and hollow fiber flow field-flow fractionation (HF5) and compared to data obtained for reference particles as well as data from electron microscopy, the standard sizing technique used in metallurgy today. AUC and HF5 provide high-quality size distributions, average over large particle numbers that enables statistical analysis, and yield useful insights for alloy design; however, DLS fails due to a lack of resolution. Important aspects in the conversion and comparison of size distributions obtained for broadly distributed particle systems with different measurement principles and the role of surfactants used in sample preparation are discussed.

1. Introduction

Microalloyed steels provide greater mechanical strengths than regular low-carbon steels at the same good weldability. They are alloyed with small amounts of Nb, Ti, and/or V at below 0.1 % by weight. These microalloy elements precipitate during the thermomechanically controlled rolling process (TMCP) as metal carbide, nitride, and/or carbonitride particles.[1,2] The particle size and the time of precipitation during TMCP affect the microstructure of the steel and hence its mechanical properties.

The first particles containing microalloy elements precipitate after casting while the slab cools down. For hot forming, the cool slab is then reheated. Reheating prior to rolling dissolves a large fraction of the initially formed particles. Some of the larger particles with diameters on the order of 300 nm resist dissolution and pin grain boundaries, thus preventing austenite grain coarsening. In the subsequent rolling process, particles with diameters of roughly 50 nm precipitate in highly deformed austenite grains and retard recrystallization. During the subsequent accelerated cooling, small particles with sizes below 10 nm form that increase the mechanical strength by precipitation hardening.[3,4] It is useful to know the distributions of precipitate particle size (particle size distribution, PSD) and composition (particle composition distribution, PCD) in microalloyed steels for several reasons. First, correlations between the distributions and the material properties of steel improve the fundamental understanding of the steels and show the potential for improvement. Second, correlations between the distributions and process conditions guide the development of TMCP and lead to better materials. Finally, microalloy elements are expensive, and a better understanding of their role avoids unnecessary or inefficient addition of them.

Standard metallographic precipitate analysis uses transmission electron microscopy (TEM) on electron transparent foils or carbon extraction replicas for the detailed analysis of Nb, Ti, and V carbonitride particle size and morphology. Information on the chemical composition is accessible through energy dispersive X-ray analysis (EDX), electron energy loss spectroscopy (EELS), and selective area diffraction (SAD). The sample volumes that can be probed with such methods are limited to the

Dr. A. Hegetschweiler, Dr. A.-R. Jochem, Prof. T. Kraus
INM- Leibniz Institute for New Materials
Campus D2 2, 66123 Saarbrücken, Germany
E-mail: tobias.kraus@leibniz-inm.de
A. Zimmermann, Prof. T. Kraus
Colloid and Interface Chemistry
Saarland University
Campus D2 2, 66123 Saarbrücken, Germany
Dr. J. Walter
Institute of Particle Technology (LFG)
Friedrich-Alexander-Universität Erlangen-Nürnberg (FAU)
Cauerstr. 4, 91058 Erlangen, Germany
Dr. T. Staudt
AG der Dillinger Hüttenwerke
Werkstraße 1, 66763 Dillingen, Germany

The ORCID identification number(s) for the author(s) of this article can be found under https://doi.org/10.1002/ppsc.202000236.

DOI: 10.1002/ppsc.202000236

order of 10 μm^3.[5] The number of particles that can be analyzed by electron microscopy, for example, generally ranges from 100 to 1000.[6,7] The reconstruction of complex PSDs, however, commonly requires the analysis of more than 10^4 particles in order to be statistically relevant and provide sufficient resolution.[8]

The introduction of the matrix dissolution technique was an important step towards high-resolution PSDs of precipitates. The precipitates are extracted from the steel chemically or electrolytically, purified, and subsequently analyzed.[9–12] This increased the probed volume to above 0.1 cm^3 and the number of accessible particles to more than 10^8. The resulting dataset is large enough to average over many grains, avoid a bias due to local microstructure, and to provide statistically sound PSDs even of broad distributions. Sizing the extracted particles became the limiting step. The initial studies on matrix dissolution used electron microscopy on precipitates dried on TEM grids, which increased the areal density that could be observed microscopically by at least 2–3 times over the traditional carbon replicas, but still required time-consuming sizing via image analysis. Manual counting of hundreds of particles in such micrographs typically requires one day. Improved automatic image analysis will probably accelerate this, but the number of particles remains fundamentally limited by TEM sample preparation and imaging.

Here, we evaluate bulk colloidal sizing techniques for precipitate analysis. Matrix dissolution can provide a stable, colloidal suspension of precipitate particles in a liquid.[9] We believe that it is accessible to well-established colloidal sizing methods that provide PSDs[13–15] based on the order of 10^{11} particles.[16] The colloids formed in matrix dissolution are a challenging case for particle system characterization because concentrations are low, particle shapes are complex and much of the mass is concentrated in large particles, even though a large number of small particles strongly affects the steel's properties and needs to be correctly recorded.

The purpose of this contribution is to assess which colloidal sizing techniques provide a good compromise between methodological complexity and data quality. For example, ensemble techniques such as dynamic light scattering (DLS) that average over a large number of particles are easy to use but often fail to reconstruct broad PSDs.[13,14] Counting or fractionating methods are more complex but provide greater resolution.[13–17] A universal rule for the choice of method does not exist because the methods react differently to the particle systems in question. We analyzed precipitate suspensions using DLS, analytical ultracentrifugation (AUC), and hollow fiber flow field-flow fractionation (HF5). The methods were selected because they are suitable for the required size range, available as commercial instruments, and sufficiently common to be available at least in specialized laboratories.

Particles extracted from the same steel were analyzed using all three methods to assess which sizing principle is more suitable.[18] We chose common microalloyed steels for this evaluation, one containing only Ti, the second both Nb and Ti. Two alloy elements can lead to more complex PSDs since the solubilities of their nitrides and carbides differ and they may form heterogenous particles.

A surfactant (Disperbyk-2012) was added during extraction. We recently introduced this step to the matrix dissolution technique in order to reduce particle loss, agglomeration, and limit the formation of unwanted silicate networks that impede analysis.[9] The surfactant achieves this by forming a shell that needs to be considered when analyzing colloidal sizing data and extract data on the particle core as it was present in the steel. We used reference particles in order to estimate the thickness and density of the shell. Well-defined reference particles of Nb and Ti carbonitrides are not available; we used Au nanoparticles with narrow size distributions (less than 15 percent standard deviation of the mean diameter) coated with Disperbyk-2012 and analyzed them via DLS, TEM, and AUC to obtain the thickness and density of the shell.

The comparison of PSDs from different methods requires caution. Sizing can be based on different particle properties; their conversion into core diameter PSDs is based on models with assumptions that cause uncertainty. For example, TEM and XRD only provide the inorganic core diameter, while DLS, AUC, and HF5 provide the hydrodynamic diameter or the sedimentation equivalent diameter and are sensitive to soft surfactant shells.[19,20] The level of uncertainty is usually a function of particle size. For small particles, the surfactant shell can constitute a large part of the particle. The PSD is weighted according to the measured quantity. Counting analysis of TEM micrographs, for example, provides number-weighted distributions while DLS provides intensity-weighted distributions. The abundance of a particle with the radius r then scales with r^6 ($I \propto r^6$), so that larger particles are distinctly more heavily weighted than in the corresponding number-weighted distribution.[19,20] Conversion between different weightings is challenging for the complex particle systems found in steel. We show the effect of different weightings qualitatively and discuss to which extent the data from different methods can be compared.

This article is structured as follows: First, we briefly introduce the extraction of Nb and Ti carbonitride particles from microalloyed steels by acidic dissolution of the steel sample using published techniques.[9] Results from TEM analysis of the particles are then introduced and compared with the PSDs obtained from the colloidal approaches, namely DLS, AUC, and HF5. All methods except DLS were able to distinguish the monomodal PSD of particles in one steel type from the bimodal PSD of particles in the other steel and found particle size maxima in the same size ranges. We compare the methods and discuss their suitability for the analysis of particles from microalloyed steels. We show that both AUC and HF5 provide data from a large number of particles and the results are comparable to those obtained from TEM. Both AUC and HF5 are affected by the surfactant shell formed during extraction and we discuss how to consider it using reference particles.

2. Results and Discussion

2.1. Transmission Electron Microscopy

Figures 1a and d are TEM micrographs of the particles extracted from microalloyed steels. The spacing between the dried particles suggests good initial dispersion with little agglomeration. The weak shadows are caused by remaining dispersant and residues of $Fe(OH)_x$ and $Si_xAl_yO_z$ that were not completely removed during centrifugation. The shapes of the particles extracted from Steel A varied broadly from spherical to angular geometries. Steel B mainly contained particles with cubic and

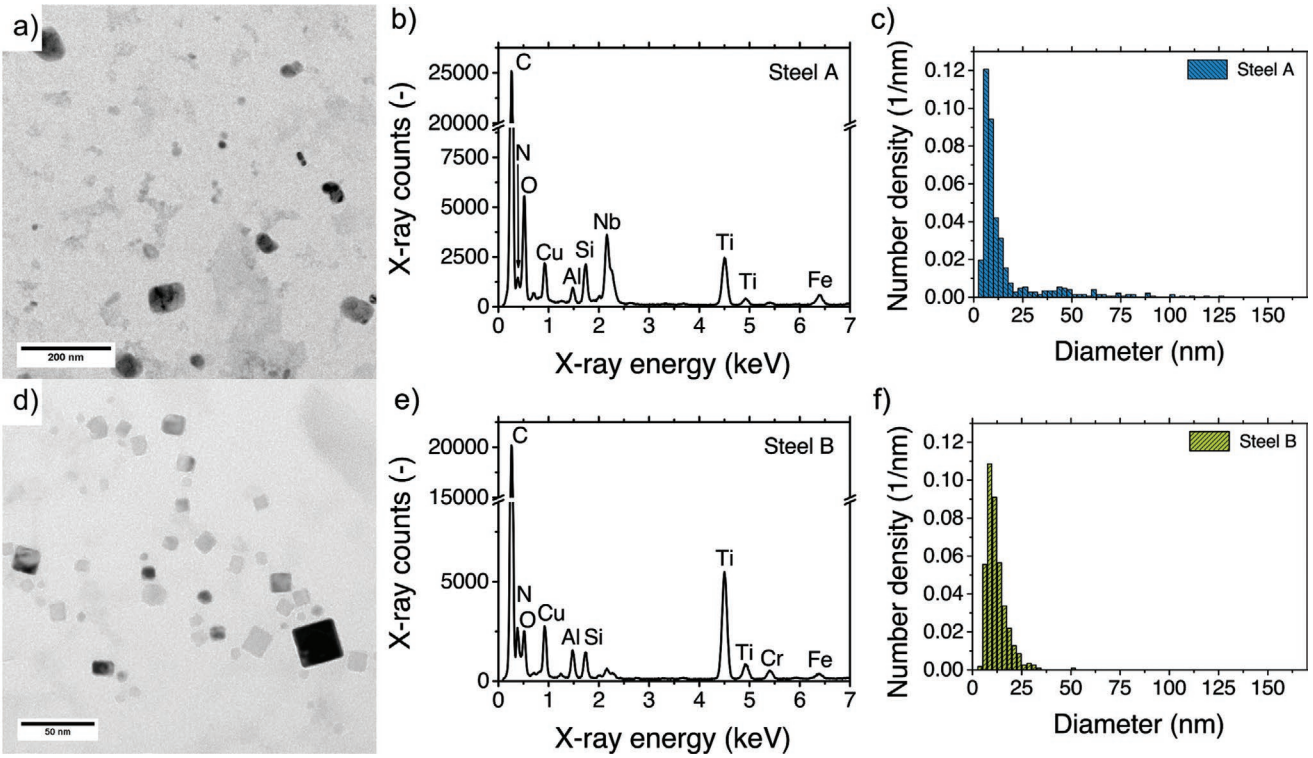

Figure 1. TEM characterization of precipitate particles extracted from Steels A and B: a) Overview of particles from Steel A. b) EDX spectrum of a) averaged over the entire area. c) PSDs obtained through image analysis of 590 particles extracted from Steel A. d) Overview micrograph for particles from Steel B. e) EDX spectrum of d). f) PSD from image analysis of 475 particles of Steel B.

cuboid shapes. The EDX spectra averaged over Figure 1a and d are shown in Figure 1b and e, respectively.

The EDX spectra indicate particles containing Nb and Ti. Particles from Steel A contained both Ti and Nb. In general, a well-known particle formation mechanism starts with the precipitation of Ti as TiN at high temperatures. The TiN particles act as nuclei for NbCN, which overgrows them at lower temperatures and forms "core-shell particles". The large particles in Steel A therefore usually contain Ti and Nb. Other elements present are Al, Si, and O, which are contained in the surrounding residue. Steel B mainly contains Ti(C)N particles. There are also traces of Al, Si, O, and Fe, which we attribute to contaminations from the matrix.

Image analysis of the TEM micrographs leads to the number-weighted PSDs shown in Figure 1c and f. Steel A contained a broad distribution of particles with a particle population in the diameter range of 5 nm to 10 nm and fewer, larger particles in the range of 20 nm to 80 nm. Steel B had a monomodal PSD with a modal diameter of approximately 10 nm.

2.2. Dynamic Light Scattering

DLS using monochromatic laser illumination led to autocorrelated scattering data that contains information on the PSD. Different algorithms have been developed (and implemented in commercial instruments) for the analysis of the autocorrelation function. A succinct overview is available by Hassan et al.[21] Several popular algorithms (e.g., the so-called "cumulant fit" that we used for the analysis of Au reference particles) assume a monomodal particle distribution. Other algorithms (e.g. CONTIN or NNLS that we used for the analysis of the particles extracted from steel) can reconstruct the overall PSD as far as possible given the indirect measurement.[22]

Figure 2 shows the intensity-weighted particle size distribution for Steel A and Steel B from NNLS analysis. The method indicated a monomodal diameter distribution ranging from 50 nm to 300 nm for Steel A with a maximum at approximately 100 nm and a similar monomodal distribution for Steel B between 70 nm to 400 nm. Both PSDs had clear maxima.

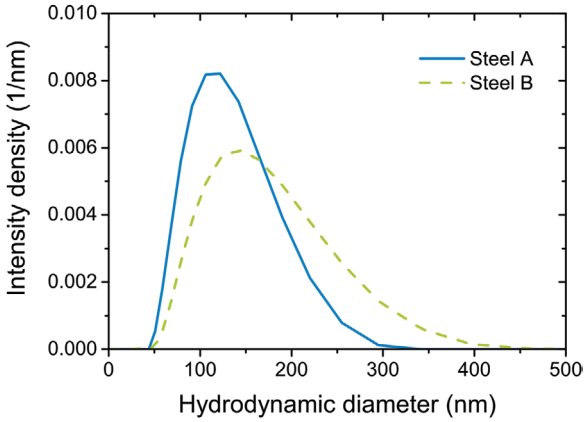

Figure 2. DLS of particles extracted from Steel A and Steel B. Each value is an average of three individual measurements.

There is a clear, qualitative difference between the DLS results and the PSDs from TEM, AUC, and HF5 (see below). Most notably, DLS did not indicate the bimodal distribution of Steel A. This is a well-known limitation of DLS as large particles scatter light far more strongly than small particles. The relation for spheres in the Rayleigh scattering regime $\left(d < \frac{\lambda}{10}\right)$ is

$$I = I_0 \frac{1+\cos^2\theta}{2R^2}\left(\frac{2\pi}{\lambda}\right)^4\left(\frac{n^2-1}{n^2+2}\right)^2 r^6 \quad (1)$$

with the scattered intensity I, the intensity of the incident light I_0, the refractive index n, the distance to the particle R, the scattering angle θ, the wavelength of the incident light λ, and the particle radius r. The overall scattering signal of a broadly distributed suspension is therefore dominated by the largest particles, while the scattering from smaller particles is so weak that it cannot be detected at all or at least not be autocorrelated. Additional problems of multiple scattering and the noise from other sources that would not be present if there were only small particles may contribute.

A second consequence of Equation 1 is the weighting of PSDs from DLS. Particle size distributions measured with DLS are intensity-weighted size distributions as shown in Figure 2 with intensities that are proportional to the sixth power of the particle radius. A direct comparison to PSDs measured with other sizing techniques require a transformation to e.g. volume-weighted or number-weighted distributions. Equation 2 describes the transformation from an intensity-weighted PSD ($q_6(r)$) into a number-weighted PSD ($q_0(r)$):

$$q_0(r) = \frac{r^{-6} q_6(r)}{\int_{r_{min}}^{r_{max}} r^{-6} q_6(r) dr} \quad (2)$$

This transformation cannot remove the uncertainties of the DLS measurements that strongly depend on the particle diameter and are most pronounced for the smallest particles. Noise in the small-particle part of the PSD is magnified in this transformation and may create misleading PSD features. Weak scattering from small particles that has not been detected will not be reflected in the transformed PSD even if the number of small particles is large. Transformation requires assumptions on particle shape and refractive index, too; both are not known for the particles used here. Nevertheless, we show number-weighted PSD that were obtained by transformations with reasonable assumptions on the refractive index in the SI to enable a comparison of same weighted PSDs.

We conclude that DLS is not suitable for the analysis of non-fractionated particle suspensions extracted from steel because the largest particles dominate the scattering signal clearly and the scattering signal of the smaller particles is not detected. Further, the transformation of the intensity-weighted distribution requires data on the particles that is not available in this case.

2.3. Analytical Ultracentrifugation

AUC is a fractionating particle sizing method for broad and multimodal particle systems.[23–27] It is based on the measurement of sedimentation properties of the particles under high centrifugal forces. Most common is the sedimentation velocity (SV) experiment where the particles' positions are reconstructed from optical transmission as a function of time and space in the measurement cell. The measurement provides the sedimentation coefficient s, which can be transformed into the sedimentation equivalent particle size x_{sed} by

$$x_{sed} = \sqrt{\frac{18\eta_s s}{(\rho_p - \rho_s)}} \quad (3)$$

with the particle density ρ_p, solvent density ρ_s, and solvent viscosity η_s.

The particle size distribution $g(x_{sed})$ was obtained from the sedimentation coefficient distribution $g(s)$ by:

$$g(x_{sed}) = g(s)\frac{ds}{dx_{sed}} = g(s)\frac{x_{sed}(\rho_p - \rho_s)}{9\eta_s} \quad (4)$$

SV experiments were performed on the extracted particles. **Figure 3**a and b depicts the sedimentation coefficient distributions measured at wavelengths of 280 nm, 350 nm, 400 nm, 450 nm, 529 nm, and 620 nm by the multiwavelength AUC. Note the logarithmic scaling of the sedimentation coefficient axis.

Particles from Steel A had a very broad, bimodal sedimentation coefficient distribution ranging from ≈ 20 S to 70000 S with maxima at about 600 S and 8000 S. Particles extracted from Steel B had sedimentation coefficients ranging from ≈20 S to 5000 S with one maximum at about 300 S to 600 S, depending on the wavelength. The shape of the distributions strongly depends on the wavelength used for the turbidity measurements in both cases.

The transformation of the sedimentation coefficient distributions into PSDs requires assumptions on the thickness and the density of the surfactant shell that is introduced during the extraction process, on particle shape, and on particle composition. The average density of the particles that sets the sedimentation coefficient is affected by the particle composition and the surfactant shell. The shell strongly affects small particles with diameters on the order of 10 nm. The error in size calculation without corrected density for such particles is about 20%. We performed this correction for each particle size by determining an effective particle density:[28]

$$\rho_p = \rho_{shell} + \left(\frac{(x_{sed} - 2t_{ligand})^3}{x_{sed}^3}\right)(\rho_{core} - \rho_{shell}) \quad (5)$$

with the corrected particle density ρ_p, the density of the organic ligand ρ_{shell}, the bulk density of the inorganic particle core ρ_{core}, the thickness of the organic ligand t_{ligand}, and the sedimentation equivalent diameter x_{sed}. Herein, it is assumed that the particles are spherical, hence, x_{sed} equals the hydrodynamic diameter x_h.

The thickness of the surfactant shell was estimated using Au reference particles that we coated with Disperbyk-2012 (see methods section and supporting information). The hydrodynamic diameter of coated and uncoated reference particles with

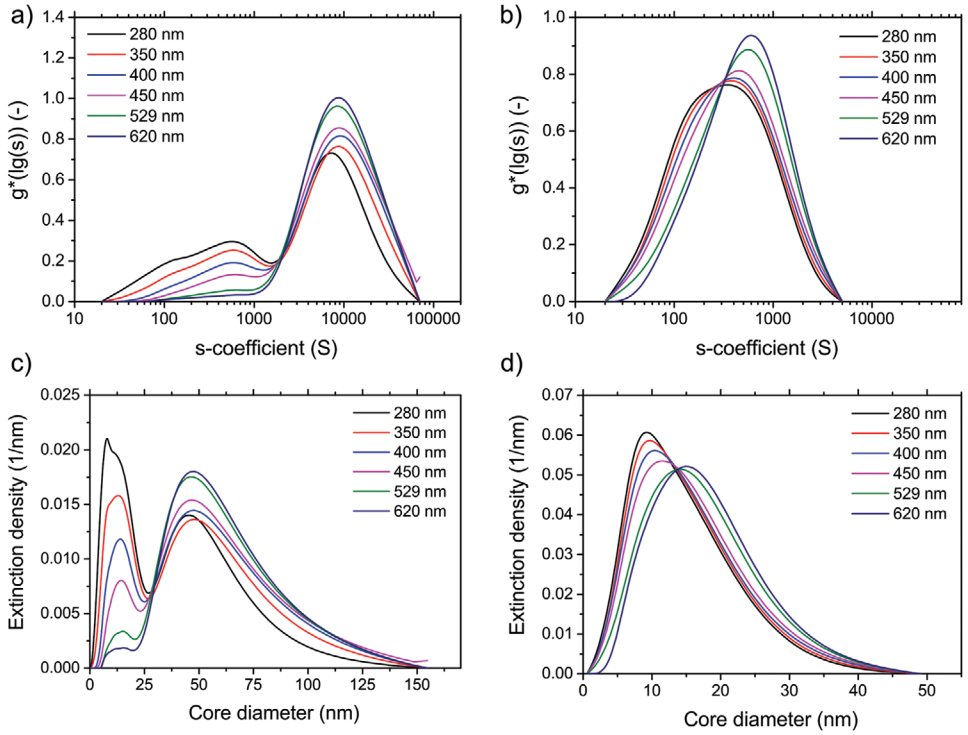

Figure 3. AUC characterization of precipitate particles extracted from Steels A and B: Non-normalized sedimentation coefficient distribution of a) Steel A and b) Steel B and the corresponding normalized extinction-weighted PSDs for c) Steel A and d) Steel B. The density of bulk NbTiCN was assumed for particles from Steel A and the density of bulk TiN was used for Steel B.

different core sizes were determined using DLS, plotted against each other, and extrapolated to a core diameter of zero. This led to an estimated shell thickness of 5.6 nm. We performed a second experiment to estimate the thickness and the density of the surfactant shell using AUC and TEM. The PSDs of differently sized, surfactant-coated Au reference particles were obtained from SV experiments in AUC. Because we know the core diameter of the Au particles precisely, we could then fit thickness and density of the surfactant shell using least squares minimization, which led to a density of 1.25 g cm^{-3} and a shell thickness of 5.7 nm, that we used for all further derivations of the core sizes. Note that the properties determined for the surfactant shell on Au particles may deviate from the properties of the shell on the steel particles to a degree. However, zeta potential measurements indicated that the shells were similarly charged. The shell thickness obtained for the reference particles will therefore serve as a good estimate of the true surfactant shell thickness. Uncertainties in the shell thickness and its distribution on the complex steel particles does introduce uncertainties into the comparison of TEM, AUC, and HF5, however. Section 2.5 and the SI provide further details.

The core density was estimated based on metallurgical considerations. The mutual solubility of the microalloy carbonitrides leads to precipitates with core densities between that of NbC (ρ_{NbC} = 7.8 g cm^{-3}), NbN (ρ_{NbN} = 7.3 g cm^{-3}), TiC (ρ_{TiC} = 4.9 g cm^{-3}), and TiN (ρ_{TiN} = 5.4 g cm^{-3}).[29] The precipitates may have compositions in the entire range of $Nb_wTi_xC_yN_z$ and contain vacancies in the crystal lattice that affect their density. Steel A was alloyed with Nb and Ti, thus we used the arithmetic mean of the densities of NbC and TiN (6.6 g cm^{-3}) as a simple estimate. Note that TMCP theory predicts that a fraction of small particles of pure NbC should form, too. We therefore expect reduced accuracy for the PSD at smaller particle sizes. Steel B contained only Ti, hence we estimated the density of the precipitates to be 5.4 g cm^{-3}, the bulk density of TiN.

The normalized extinction-weighted PSDs calculated using above assumptions are shown in Figure 3c and d for Steels A and B using data obtained at wavelengths of 280 nm, 350 nm, 400 nm, 450 nm, 529 nm, and 620 nm. The distributions show the core diameters with twice the thickness of the surfactant shell (11.4 nm) subtracted from the measured sedimentation equivalent diameter. The local relative frequencies of the PSDs differed significantly depending on the measurement wavelength, but the overall distributions remained virtually constant. The maxima of the PSD for Steel A were at diameters ≈ 10 nm to 15 nm and at 50 nm for all wavelengths. The minimum between the two peaks was at ≈ 20 nm. The large particle fraction had sizes up to 150 nm. The maximum of the PSD of Steel B was at ≈ 10 nm to 15 nm with largest particles ≈ 50 nm.

The dependence of the sedimentation factors and PSD on wavelengths is most likely due to the wavelength-dependent extinction of the surfactant shell that mainly absorbs light in the UV range (up to ≈ 350 nm to 400 nm). This strongly affects small particles, where the shell accounts for a large proportion of the volume. The observed extinction of these particles at short wavelengths is higher than at longer wavelengths, and their concentration is overestimated. It is difficult to correct this effect and advisable to compare measurements at

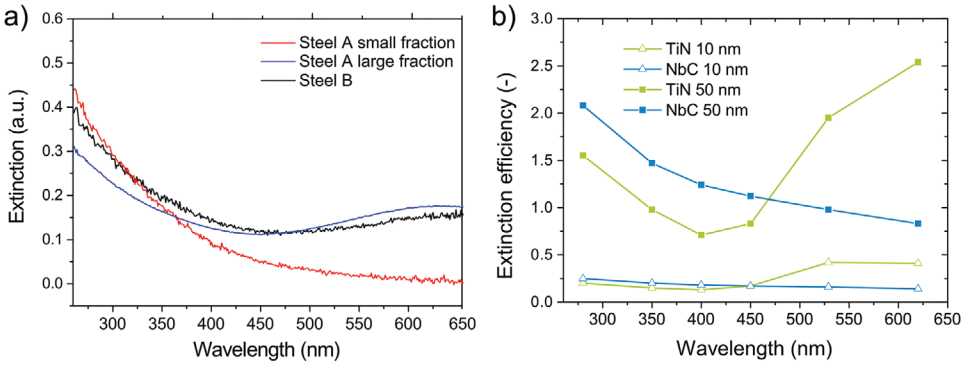

Figure 4. Particle fraction dependent extinction: a) Extinction spectra of the individual particle fractions. b) Calculated extinction efficiencies for TiN and NbC particles with sizes of 10 nm and 50 nm.

different wavelengths to verify AUC results. We can even exploit the wavelength dependency of the AUC data in order to gain at least qualitative information on the composition of the particles in different parts of the PSD.

Next, we consider **Figure 4**a that shows optical spectra for the larger and smaller sized particle fractions of Steel A and the particles of Steel B. The extinction of all particles initially drops with increasing wavelength. This is caused by the particle core as well as the surfactant shell as discussed above. The optical extinction of the large particle fraction from Steel A, however, increases again at longer wavelengths, which cannot be caused by the shell. Regarding the calculated extinction efficiency in Figure 4b, that is defined as the extinction cross section normalized to the particle cross section, an increase in extinction is to be expected for TiN particles at wavelengths above 500 nm, but not for NbC particles. We conclude that the large particle fractions from Steel A and the particles in Steel B contain TiN, while the small particle fraction from Steel A contains only NbC. The TEM/EDX results discussed above confirm this reasoning.

2.4. Field-Flow Fractionation

Field-flow fractionation (FFF) exploits a liquid flow to fractionate multimodal particle mixtures.[30] It is a chromatography-like technique that relies on particle separation in an external force field that is applied perpendicular to the main flow direction.[31] The nature of the external force field determines the separation mechanism. In the most common technique, Flow FFF, particles are separated depending on their diffusion coefficient by a laminar cross-flow that pushes the particles against a membrane.

Extracted particles from both steels were analyzed with HF5, which uses a hollow fiber as separation channel. Retention times (the times it takes the particles to pass through the separation channel) were recorded using an in-flow UV-Vis detector at a wavelength of 280 nm (**Figure 5**a). The wavelength was chosen because it provided the strongest signal and allowed the detection of small particles below approximately 15 nm. Other detectors coupled with the FFF channel include online DLS or multiangle static light scattering (MALS). These detection systems were tested, too, but did not provide useful data, for the smallest species in the samples. The measured retention time distribution was transformed into a hydrodynamic PSD using a calibration function obtained from the Au nanoparticles and Equations 5 and 6 in the supporting information. We subtracted the thickness of the surfactant shell (as obtained from AUC, see above) from the hydrodynamic diameter. Figure 5b illustrates the extinction-weighted PSDs of the particle core for Steel A and Steel B.

The fractograms from HF5 indicate good separation of the particles. The void peak at 5.92 min occurs in all HF5 experiments and is used to determine the effective net retention time.

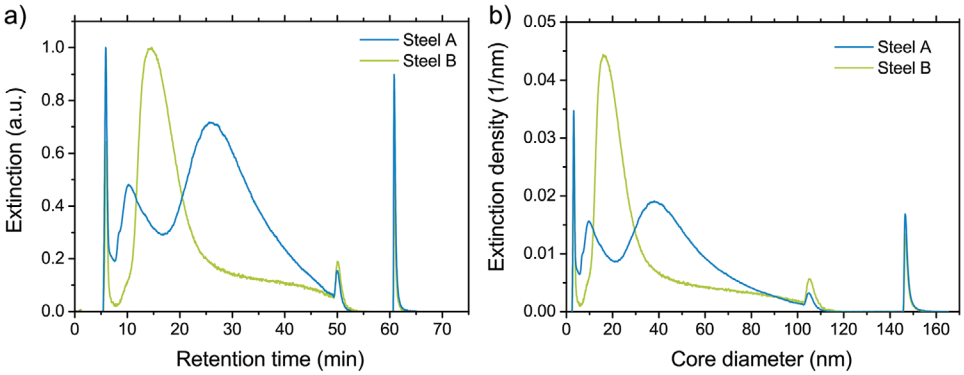

Figure 5. HF5 characterization of precipitate particles extracted from Steel A and Steel B: a) Retention time of extracted particles. b) Calculated particle core diameter.

The release peak at ≈ 50 min indicates that the cross-flow has been switched off. It is caused by particles that remained at the membrane and finally left the channel.

Retention time analysis on the particles extracted from Steel A indicated a bimodal size distribution with maxima at approximately 10 nm and at 40 nm. Steel B contained particles with a monomodal size distribution with a maximum at 17 nm. It is likely that the optical extinction of the surfactant shell leads to an overestimated frequency of smaller particles as discussed for AUC above. We still consider measuring at 280 nm the best choice, because the prominent extinction of the surfactant provides a sufficiently strong UV-vis signal. The HF5 technique leads to a 1000-fold dilution of the sample that impedes the detection of small particles. We found that large particles could be readily detected at longer wavelengths, too, with small shifts in retention time but smaller particles did not provide extinction above the background noise. Other detection schemes based on light scattering (DLS, MALS) worked for the larger particles, too, but did not provide useful data on smaller particles.

2.5. Comparison of Particle Size Distributions

The PSDs derived from AUC, HF5, and TEM are compared in **Figure 6**. The plots illustrate AUC and HF5 data obtained at a detection wavelength of 280 nm to minimize the spectral effects discussed above. The void peak in the HF5 measurement was excluded in Figure 6 for clarity and ease of comparison with other methods. The void peak contained particles that were not retained and therefore not properly separated according to their size during the experiment. The position or shape of the peak does not contain any information about the sizes of the particles. The overall amount of particles contained in the peak was small enough not to cause deviations in the main part of the elugram. We excluded the void peak in Figure 6 to enable a better comparison of the the different sizing methods.

The PSDs found by the different methods were similar. For Steel A, all three methods found distributions with a smaller diameter fraction of around 10 nm and a larger diameter fraction with diameters ranging from 20 nm to 100 nm. For Steel B, the analyses indicated a monomodal distribution with a diameter of approximately 10 nm to 15 nm. The smaller particles in Steel A were hardly discernible compared to the larger particles in TEM but could be easily detected by AUC and HF5. The relative frequency of the individual populations in TEM was very different from both other methods although the average sizes of all fractions is similar in TEM, AUC, and HF5. The overall size distributions were slightly shifted even between the two colloidal methods.

First, consider the differences between TEM and the two colloidal sizing techniques, AUC and HF5. Both AUC and HF5 provide extinction-weighted data, while the PSD from TEM is number-weighted. It is theoretically possible to convert the distributions, but this requires an optical model based on the refractive index, shape, composition, and morphology of the particles. Given that the analyzed particles differ in shape, composition, and refractive indices and carry a surfactant shell, such conversion is associated with large uncertainties.[32] We therefore recommend to report extinction-weighted data when using AUC and HF5. The resulting PSDs are useful for the qualitative analysis of the size distributions, because the optical properties are unlikely to introduce misleading features. A qualitative comparison of number- and extinction-weighted PSDs is straightforward for monomodal systems such as that of Steel B. One of the most important applications of such PSDs is the improvement of the alloy composition and steel processing. We recommend directly comparing the extinction-weighted PSDs from steels with changed composition or processing conditions rather than converting them to number-weighted PSDs. The supporting information contains a direct comparison of the number-weighted data from all three methods and highlight the uncertainties that are caused by the y axis transformation. The comparison highlights uncertainties on the ligand shell thickness that are used in the calculation of the particle core size for AUC and HF5. Note that the overall congruence of the independent sizing methods is good. We once again caution that the necessary transformations magnify uncertainties; the relative reliability of the different methods depends on particle size in the combined plots.

A second important origin of differences between PSDs from TEM and colloidal methods are the large differences in analyzed particle numbers. For TEM, the number of counted particles is around 500 for both steels. In contrast, AUC investigated a sample volume of ≈400 µL, and the injected sample volume in HF5 was ≈50 µL. Assuming a mass concentration of 6 mg L^{-1} and a mean particle size of 50 nm, this corresponds to a number of particles on the order of 10^9 for HF5 and 10^{10} for

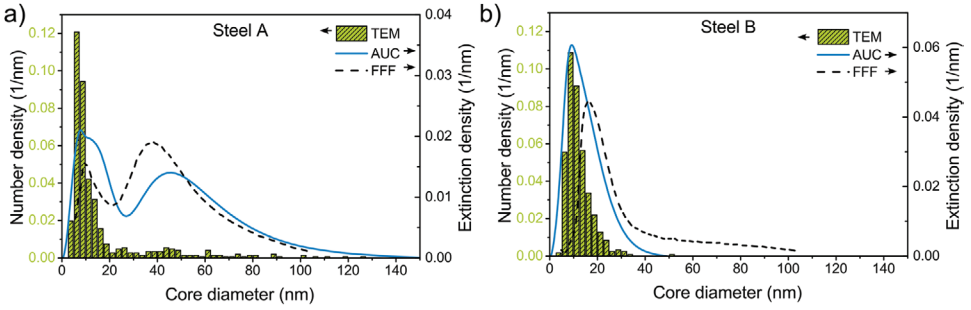

Figure 6. PSDs from TEM (number density), HF5, and AUC (both extinction density) for a) Steel A and b) Steel B. The detection wavelength for AUC and HF5 was 280 nm. The void peak (retention times below ≈ 6 min) was excluded in this image. The void peak consists of unretained particles that do not contribute to the particle size distribution.

AUC. This explains the increased resolution of the PSDs from AUC and HF5. That is particularly beneficial for the larger particle fraction in Steel A, that suffers from low particle counts in TEM analysis. Additionally, both methods clearly reveal the smaller particle fraction in Steel A that may be quite hard to detect using TEM because of the weak contrast compared to larger particles. It is a clear benefit of the colloidal approach.

Finally, we observe a shift in the PSDs measured with AUC and HF5. This shift in the PSDs probably occurs due to the different separation principles of the methods and the assumptions made for the calculation of the particle core sizes. Particle fractionation in HF5 only depends on diffusion and thus on the hydrodynamic diameter, while in AUC, it is affected by the density of the particles, too. In precipitates from steel, composition is heterogeneous and density varies. Further assumptions need to be made for the ligand shell. Over- or underestimation of the overall particle density leads to a shift in the calculated particle sizes. A variation in particle densities leads to an artificial broadening of the particle fractions. The particles' shapes affect their friction coefficient in fluid flow and thus impact the derived diffusion and sedimentation coefficients.[33,34] For cubic shapes, the diffusion coefficient is smaller compared to spherical particles. In HF5, where diffusion is the principal separation mechanism, these particles thus appear to be larger (especially for Steel B). In AUC, however, particles with higher densities (as we have them here) are dominated by their sedimentation during AUC experiments, while diffusion is less important or negligible. This may lead to differences in the measured PSD, that are larger the more the assumed particle density deviates from the real particle density. All this affects HF5 and AUC and produces also an uncertainty in the particle size distribution compared with TEM.

3. Conclusion

Recent progress in chemical extraction has made it possible to extract precipitates from steel and analyze them as colloidal dispersions. We show here that analytical ultracentrifugation (AUC) and hollow fiber flow field-flow fractionation (HF5) are suitable to analyze a statistically meaningful number of precipitates in such suspensions. It thus becomes possible to analyze 10^9 particles in a single step, which provides smooth particle size distributions over a size range from a few to several hundred nanometers.

This new type of data on precipitates in steel complements the results of well-established TEM characterization that usually analyzes particle numbers on the order $<10^3$. Colloidal particle sizing enables fast assessment of the size distribution of large particle numbers from macroscopic sample volumes. The resulting size distributions provide useful qualitative information on the influence of different TMCP production routes on precipitation. Comparison of the different particle size distributions enables the optimization of the steel production process for improved mechanical properties and reduced production costs.

Comparing the precipitate size distributions from TEM and colloidal techniques requires an in-depth analysis of the different techniques. We find that the inherent weighting of the different detection techniques and the heterogeneity in shape, composition and functionalization of the precipitates lead to complex deviations that need to be considered. The rich data obtained in AUC and HF5 experiments is not limited to size distributions. Future models of the precipitates that consider not only size, but also shape and composition could make it possible to provide more detailed precipitate analysis in a single routine step and aid material development.

Table 1. Elemental composition of the examined steels.

Element	Nb(wt%)	Ti(wt%)	Si(wt%)	CEV*(wt%)
Steel A	0.039	0.015	0.171	0.368
Steel B	0.001	0.008	0.43	0.424

*CEV = Carbon Equivalent Value

4. Experimental Section

Chemicals and Materials: All chemicals were used as purchased without further purification. Ammonium nitrate (p.a.) and sodium dodecyl sulfate (≥99%) used for HF5 analysis were bought from Sigma-Aldrich (Germany).

The etching solution was freshly prepared from concentrated sulfuric acid (Sigma Aldrich, 95–97%, p.a., Germany) by diluting with ultrapure water (>18 MΩ cm) (Milli-Q water purification system type Advantage A10 and ELIX 20, Millipore Corp., USA). The dispersant used in the etching solution was Disperbyk-2012 (Byk additives and instruments, Germany). Two different microalloyed steel samples (denoted "Steel A" and "Steel B") were analyzed; they had the compositions given in **Table 1**.

Citrate-stabilized Au nanoparticles with nominal diameters of 5, 20, 50, and 80 nm were purchased from nanocomposix (San Diego, USA), and AuNP with a diameter of 30 nm were purchased from nanopartz (Loveland, USA). Particles with a nominal diameter of 15 nm were synthesized according to Frens.[35]

Gold reference particles stabilized with Disperbyk-2012 were prepared by a ligand exchange of citrate-stabilized AuNP with Disperbyk-2012. Citrate-stabilized AuNP (1.5 mL) were added to Disperbyk-2012 (15 mg) and the particle suspension was shaken for 24 h. To remove the excess surfactant, the particles were centrifuged (Centrifuge 5418, Eppendorf, Germany) and the supernatant was replaced with Milli-Q water in three washing cycles. The zeta potentials of the resulting particles were then measured and compared to those of Nb and Ti carbonitride particles after extraction. Similar values as shown in **Table 2** were found.

Extraction: Nb carbonitride and Ti carbonitride particles were extracted from microalloyed thermomechanically rolled pipeline steels (Steel A and Steel B) by dissolution of the iron matrix.[9] For each steel, a sample (1 g) was dissolved in sulfuric acid (0.05 L, 0.5 mol L^{-1}) containing Disperbyk-2012 (0.1 vol%). The etching solution was heated to 70 °C and stirred at 200 rpm. After dissolution was complete, the particle suspension was sonicated for 1 min in an ultrasonic bath (Elma X-tra 50 H, 160 W, Germany). The sample was split in two 25 mL aliquots and diluted with water to 35.5 mL for centrifugation in an ultracentrifuge

Table 2. Zeta potential of Au reference particles before (citrate stabilized) and after (Disperbyk-2012) ligand exchange and of extracted particles from Steel A and Steel B.

Ligand	Au5 [mV]	Au15 [mV]	Au20 [mV]	Au50 [mV]	Au80 [mV]	Steel A [mV]	Steel B [mV]
Citrate	−42	−47	−50	−56	−58	–	–
Disperbyk	−20	−20	−25	−23	−30	−26	−33

(XL-I 70 K, Beckman-Coulter, Germany) at 504 000 rcf and 20 °C for 90 min. The supernatant was removed (30 mL) and replaced by Milli-Q water. Washing and centrifugation were repeated seven times to remove the dissolved iron. In the final step, as much supernatant as possible was removed after centrifugation to obtain a high particle concentration of approximately 6 mg L^{-1}. This procedure allowed the authors to extract a large amount of particles. Losses from particle etching and insufficient sedimentation during centrifugation could not be completely excluded, however. Previously the particle losses caused by etching of particles were studied in ref. [9]. The amounts of ionic Nb and Ti in the supernatant are useful as indicators of the extent to which particles were etched; 5% of the total alloyed Nb and 20% of the total alloyed Ti were detected in the supernatant. A mass reduction of 20% by etching would result in a size reduction of approximately 5–10%. It was likely that very small particles were etched most due to their large surface-to-volume area and slow sedimentation. Errors due to unwanted particle etching would therefore mainly affect the smallest particles.

Analysis—Transmission Electron Microscopy: The extracted particles were observed using a JEM-2100 microscope from JEOL (Germany) with an acceleration voltage of 200 kV. Electron-dispersive X-ray analysis (EDX) was conducted using a Noran System 7 X-ray Microanalysis System (Thermo Scientific, Germany). For sample preparation, a volume of 2.5 µL particle suspension was dried on a carbon coated copper grid. 590 particles from Steel A and 475 particles from Steel B were analyzed. The particle size was evaluated via image analysis with the FIJI software that determined the diameter of a circle of the same area for each particle.[36]

Analytical Ultracentrifugation: A preparative ultracentrifuge (Optima XL-80K, Beckman-Coulter, USA) modified with transmission optics and a multiwavelength detector[23,37] was used for sedimentation velocity (SV) experiments. Two-sector titanium centerpieces (Nanolytics, Potsdam, Germany) were used for all experiments. The samples were centrifuged at a temperature of 20 °C and velocity of 5000 rpm. SV data were recorded with a maximum possible data collection rate with one recording every 2 min. Data analysis was performed using the ls-g*(s) method implemented in Sedfit.[38] It determines the apparent sedimentation coefficient distribution $g^*(s)$ by direct least-squares boundary modeling and it is suitable to analyze polydisperse systems where the sedimentation coefficients span orders of magnitude.[39,40] 300 and 290 scans were evaluated for Steel A and B, respectively. Raw data and applied fits and residuals are shown in Figure S2, Supporting Information. The MWL-AUC measures the sedimentation of the particles using all wavelengths between 250 and 700 nm. This allows the determination of the extinction spectrum for every single particle fraction using the Sedanal software.[24,41,42] Reproducibility was ensured by comparing measurements from the same steel sample obtained during different extraction processes. The results of such repeats were in good accordance with the presented results.

Hollow Fiber Flow Field-Flow Fractionation: Hollow fiber flow field-flow fractionation was performed on a Wyatt Eclipse DUALTEC Flow-FFF system (Wyatt Technology Europe, Dernbach, Germany) using a quarternary pump with an integrated degassing system and an autosampler (Agilent Technologies 1260 infinity series, Agilent, Waldbronn, Germany). A hollow fiber with a polyethersulfone (PES) membrane and an inner diameter of 800 µm was used as a separation channel (Wyatt Technology Europe, Dernbach, Germany). The channel was connected to a variable wavelength UV-VIS detector (Agilent Technologies 1260 infinity series). The detection wavelength was set to 280 nm.

The eluent was composed of 0.01 mM NaOH and 0.05 wt% SDS and was optimized for particle recovery in a preliminary study (data not shown here). The membrane was conditioned for 2 h before the actual measurements with the corresponding eluent. Blank runs were performed between each measurement to ensure complete particle elution and membrane desorption of adsorbed species.

The retention time was used to determine the PSD of particles extracted from the steels by comparison with suitable reference particles. The calibration procedure involved the analysis of the Au reference particles on the same setup and with identical parameters (see Supporting Information for details). As for AUC, measurements from the same steel sample obtained during different extraction processes were performed and the results showed good accordance with the presented data.

Dynamic Light Scattering and Zeta Potential Measurements: Dynamic light scattering and zeta potential measurements were conducted on a Zetasizer Nano ZSP (Malvern Instruments, Herrenberg, Germany) with a laser wavelength of 633 nm at a power of 10 mW. The aurocorrelated scattering signal of particles extracted from steel was analyzed using the NNLS algorithm implemented in the Zetasizer software 7.11. The NNLS algorithm is based on the inverse Laplace transformation and describes the decay of the autocorrelation function Γ using a sum of exponentials with a discrete number m of decay constants.

Au reference nanoparticles were analyzed by the cumulant fit method,[21] which fits the decay of the autocorrelation function Γ with a series expansion of a single exponential decay function. Zeta potentials were determined using laser Doppler electrophoresis and the Smoluchowski model implemented in the same software.[20]

Supporting Information

Supporting Information is available from the Wiley Online Library or from the author.

Acknowledgements

The authors would like to thank Eduard Arzt for his continuing support of the project. J.W. gratefully acknowledges funding by the Deutsche Forschungsgemeinschaft (DFG, German Research Foundation) - Project-ID 416229255 - SFB 1411. This work was financially supported by the AG der Dillinger Hüttenwerke in Germany.

Open access funding enabled and organized by Projekt DEAL.

Conflict of Interest

The authors declare no conflict of interest.

Data Availability Statement

The data that support the findings of this study are available from the corresponding author upon reasonable request.

Keywords

colloidal analysis, microalloyed steels, niobium carbonitrides, precipitate analysis, titanium carbonitrides

Received: September 4, 2020
Revised: March 1, 2021
Published online:

[1] T. Gladman, *The Physical Metallurgy of Microalloyed Steels*, Vol. *615*, Maney Publishing, Leeds, UK **1997**.
[2] I. Tamura, H. Sekine, T. Tanaka, *Thermomechanical Processing of High-Strength Low-Alloy Steels*, Butterworth-Heinemann, Oxford **2013**.
[3] K. Nishioka, K. Ichikawa, *Sci. Technol. Adv. Mater.* **2012**, *13*, 023001.

[4] J. Lu, D. Ivey, H. Henein, J. Wiskel, O. Omotoso, in *2008 7th Int. Pipeline Conf.*, American Society of Mechanical Engineers, New York **2008**, pp. 85–94.
[5] J. Lu, D. Ivey, H. Henein, *Iron Steel Technol.* **2013**, *10*, 232.
[6] M. Béreš, T. E. Weirich, K. Hulka, J. Mayer, *Steel Res. Int.* **2004**, *75*, 753.
[7] Y. Shen, C. M. Wang, X. Sun, *Mater. Sci. Eng., A* **2011**, *528*, 8150.
[8] H. Masuda, K. Gotoh, *Adv. Powder Technol.* **1999**, *10*, 159.
[9] A. Hegetschweiler, T. Staudt, T. Kraus, *J. Mater. Sci.* **2019**, *54*, 5813.
[10] A. Hegetschweiler, O. Borovinskaya, T. Staudt, T. Kraus, *Anal. Chem.* **2018**, *91*, 943.
[11] J. Lu, D. Ivey, H. Henein, in *Int. Pipeline Conf.*, Volume 42630, American Society of Mechanical Engineers, New York **2006**, pp. 635–642.
[12] J. B. Wiskel, J. Lu, O. Omotoso, D. G. Ivey, H. Henein, *Metals* **2016**, *6*, 90.
[13] C. Cascio, D. Gilliland, F. Rossi, L. Calzolai, C. Contado, *Anal. Chem.* **2014**, *86*, 12143.
[14] F. Varenne, A. Makky, M. Gaucher-Delmas, F. Violleau, C. Vauthier, *Pharm. Res.* **2016**, *33*, 1220.
[15] S. C. Brown, V. Boyko, G. Meyers, M. Voetz, W. Wohlleben, *Environ. Health Perspect.* **2013**, *121*, 1282.
[16] In a NbC nanoparticle suspension with a mass concentration of 6 mg L^{-1}, the particle number concentration for particles with a size of 50 nm is 10^{11} mL^{-1}.
[17] W. Anderson, D. Kozak, V. A. Coleman, Å. K. Jämting, M. Trau, *J. Colloid Interface Sci.* **2013**, *405*, 322.
[18] Y. Dieckmann, H. Cölfen, H. Hofmann, A. Petri-Fink, *Anal. Chem.* **2009**, *81*, 3889.
[19] F. Babick, *Suspensions of Colloidal Particles and Aggregates*, Vol. *20*, Springer, Berlin **2016**.
[20] H. G. Merkus, *Particle Size Measurements: Fundamentals, Practice, Quality*, Vol. *17*, Springer Science & Business Media, Berlin **2009**.
[21] P. A. Hassan, S. Rana, G. Verma, *Langmuir* **2014**, *31*, 3.
[22] K. Franks, V. Kestens, A. Braun, G. Roebben, T. P. Linsinger, *J. Nanopart. Res.* **2019**, *21*, 195.
[23] J. Walter, K. Löhr, E. Karabudak, W. Reis, J. Mikhael, W. Peukert, W. Wohlleben, H. Cölfen, *ACS Nano* **2014**, *8*, 8871.
[24] J. Walter, P. J. Sherwood, W. Lin, D. Segets, W. F. Stafford, W. Peukert, *Anal. Chem.* **2015**, *87*, 3396.
[25] J. Walter, W. Peukert, *Nanoscale* **2016**, *8*, 7484.
[26] K. L. Planken, H. Cölfen, *Nanoscale* **2010**, *2*, 1849.
[27] B. Demeler, T.-L. Nguyen, G. E. Gorbet, V. Schirf, E. H. Brookes, P. Mulvaney, A. O. El-Ballouli, J. Pan, O. M. Bakr, A. K. Demeler, B. I. Hernandez Uribe, N. Bhattara, R. L. Whetten, *Anal. Chem.* **2014**, *86*, 7688.
[28] J. A. Jamison, K. M. Krueger, C. T. Yavuz, J. Mayo, D. LeCrone, J. J. Redden, V. L. Colvin, *ACS Nano* **2008**, *2*, 311.
[29] H. O. Pierson, *Handbook of Refractory Carbides and Nitrides: Properties, Characteristics, Processing and Applications*, William Andrew, New York **1996**.
[30] J. Gigault, J. M. Pettibone, C. Schmitt, V. A. Hackley, *Anal. Chim. Acta* **2014**, *809*, 9.
[31] J. C. Giddings, *Science* **1993**, *260*, 1456.
[32] F. Babick, C. Ullmann, *Powder Technol.* **2016**, *301*, 503.
[33] B. Carrasco, J. G. de la Torre, *Biophys. J.* **1999**, *76*, 3044.
[34] R. Stuckert, C. S. Plüisch, A. Wittemann, *Langmuir* **2018**, *34*, 13339.
[35] G. Frens, *Nat., Phys. Sci.* **1973**, *241*, 20.
[36] J. Schindelin, I. Arganda-Carreras, E. Frise, V. Kaynig, M. Longair, T. Pietzsch, S. Preibisch, C. Rueden, S. Saalfeld, B. Schmid, J.-Y. Tinevez, D. J. White, V. Hartenstein, K. Eliceiri, P. Tomancak, A. Cardona, *Nat. methods* **2012**, *9*, 676.
[37] H. Cölfen, T. M. Laue, W. Wohlleben, K. Schilling, E. Karabudak, B. W. Langhorst, E. Brookes, B. Dubbs, D. Zollars, M. Rocco, B. Demeler, *Eur. Biophys. J.* **2010**, *39*, 347.
[38] Sedfit software, http://analyticalultracentrifugation.com.
[39] P. Schuck, P. Rossmanith, *Biopolymers* **2000**, *54*, 328.
[40] V. Mittal, A. Völkel, H. Cölfen, *Macromol. Biosci.* **2010**, *10*, 754.
[41] W. F. Stafford, P. J. Sherwood, *Biophys. Chem.* **2004**, *108*, 231.
[42] Sedanal software, http://www.sedanal.org/.

